FRONTIERS OF PHYSICS

RESEARCH ARTICLE
Volume 19 / Issue 5 / 53207 / 2024

Majorana zero mode assisted spin pumping

Mingzhou Cai[1,*], Zhaoqi Chu[1,*], Zhen-Hua Wang[2], Yunjing Yu[1], Bin Wang[1,†], Jian Wang[1,3,‡]

1 State Key Laboratory of Radio Frequency Heterogeneous Integration, College of Physics and Optoelectronic Engineering, Shenzhen University, Shenzhen 518060, China
2 College of Physics and Electronic Engineering, and Center for Computational Sciences, Sichuan Normal University, Chengdu 610068, China
3 Department of Physics, The University of Hong Kong, Hong Kong, China
*These authors contributed equally to the work.
Corresponding authors. E-mail: †binwang@szu.edu.cn, ‡jianwang@hku.hk
Received January 29, 2024; accepted April 7, 2024

ABSTRACT

We present a theoretical investigation of Majorana zero mode (MZM) assisted spin pumping which consists of a quantum dot (QD) and two normal leads. When the coupling between the MZM and the QD is absent, d.c. pure spin current can be excited by a rotating magnetic field where low energy spin down electrons are flipped to high energy spin up electrons by absorbing photons. However, when the coupling is turned on, the d.c. pure spin current vanishes, and an a.c. charge current emerges with its magnitude independent of the coupling strength. We reveal that this change is due to the formation of a highly localized MZM assisted topological Andreev state at the Fermi level, which allows only the injection of electron pairs with opposite spin into the QD. By absorbing or emitting photons, the electron pairs are separated to opposite spin electrons, and then return back to the lead again, generating an a.c. charge current without spin polarization. We demonstrate the switching from d.c. pure spin current to a.c. charge current based on both Kitaev model and a more realistic topological superconductor nanowire. Although this switching can also be induced by partially separated Andreev bound state (ps-ABS) in the topological trivial phase, it is extremely unstable and highly sensitive to the Zeeman field, which is different from the switching induced by MZM. Our result suggests that quantum spin pumping may be a feasible local transport method for detecting the presence of MZMs at the ends of a superconducting nanowire.

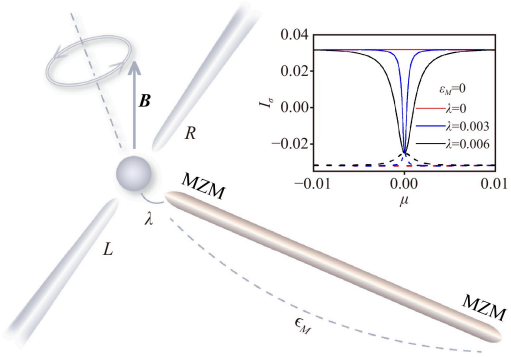

Keywords Majorana zero mode, spin pumping

1 Introduction

As a crucial component of topological materials, the topological superconductor (TSC) has attracted increasing attention both theoretically and experimentally in recent years [1–13]. TSC represents a class of superconductors with bulk pairing gaps and a pair of degenerate gapless Majorana zero mode (MZM) at the boundary or near a topological defect. An intriguing property of MZM is its non-locality along with non-Abelian braiding, which is the key to realize fault-tolerant topological quantum computing. The Kitaev model, based on a spinless p-wave superconducting chain with time reversal symmetry breaking, offers the most representative early model describing MZM [14, 15]. However, since stable p-wave

Higher Education Press

https://doi.org/10.1007/s11467-024-1407-6

superconductors with spin triplet states are rare in nature [9, 16, 17], Fu and Kane [18] proposed a more realistic implementation scheme based on the combination of a traditional *s*-wave superconductor and a topological insulator to achieve an unpaired Majorana fermion. Lutchyn *et al.* [19] and Oreg *et al.* [20] provided an experimentally feasible setting to realize one-dimensional (1D) TSC by breaking the time reversal symmetry of an atomic chain with spin–orbit coupling (SOC) due to the superconducting proximity effect. Signatures of Majorana fermions have already been found in semiconducting nanowires with strong SOC in proximity to a superconductor [21–27], and at the end of atomic iron chains on the surface of a superconductor [28, 29]. These studies provide effective methods and ideas for experimentally realizing and exploring MZMs in condensed matter physics, stimulating the rapid development of TSC in the past two decades [30–32].

Tunneling spectroscopy is a widely-used method for detecting and manipulating MZM in TSC systems. A notable feature is the appearance of a zero bias conductance peak (ZBCP), which was predicted to be $2e^2/h$ at the interface of a 1D normal metal and TSC nanowire [33]. Although the ZBCP has been observed in various semiconductor–superconductor hybrid systems [21, 28, 34], it remains a controversial criterion for confirming the presence of MZM due to alternative causes such as disorder [35–37], weak antilocalization [38] and coupling to a quantum dot [39, 40]. Recently, a $2e^2/h$ ZBCP was observed in an InSb nanowire covered with superconducting Al, demonstrating robustness to external parameters such as the Zeeman field and tunnel barrier height, thus providing definitive evidence of MZM presence [41]. Subsequently, Moore *et al.* [42, 43] pointed out that the $2e^2/h$ ZBCP may also be induced by ps-ABSs, which exists generically in the topological trivial phase of semiconductor–superconductor nanowire in the presence of Zeeman field. The authors suggested that only a nonlocal charge tunneling detection can distinguish true MZMs from ps-ABSs. However, another study found that the absence of ZBCP does not necessarily indicate the absence of MZM [44].

Since local d.c. detection of MZM always encounters difficulties, can it be detected from the perspective of a.c. transport to obtain at least some useful information? As a typical a.c. transport behavior, spin pumping has been recognized as an efficient method for generating and injecting spin into ferromagnetic/nonmagnetic material contacts [69]. The precession of magnetization caused by ferromagnetic resonance [46, 47] or acoustic waves [48–50] can drive the spin angular momentum of the ferromagnetic metal into the nonmagnetic material, creating a pure spin current without any accompanying charge current in the contact. Since spin injection relies on dynamic spin exchange rather than charge transfer, it is not affected by the impedance mismatch across the ferromagnetic/nonmagnetic material interface, and thus has a much higher efficiency than regular electron transport. Thus far, spin pumping has been extensively used for spin injection in spin sink materials, such as nonmagnetic metals [51–53], semiconductors [54, 55], and two-dimensional materials [56, 57]. Recently, spin pumping based on the Kitaev chain has been theoretically studied [58–60]. The authors have shown that MZM can be found in the absorbed power of an a.c. magnetic field at low frequencies in the resonance approximation. Unlike the parametric excitations of spin waves in ferromagnets, spin pumping in 1D topological superconductors does not produce any parametric instability. Moreover, in the dynamical regime, the frequencies of Rabi oscillations for MZM are much higher than those for gapped extended states. However, in the steady-state regime, these Rabi oscillations are blurred by relaxation processes. Very recently, spin pumping in single-subband ferrromagnetic insulator–superconducting nanowires has been theoretically investigated. It was found that the spin pumping is robustly quantized when the hybrid nanowire is in the topologically nontrivial phase. The authors suggested that observation of correlated and quantized peaks in the conductance, entropy change and spin pumping would provide strong evidence of MZMs [61].

In this study, we investigated the spin pumping effect in a two terminal quantum dot system which is coupled to MZMs at the termini of a superconducting nanowire. A constant pure spin current can be induced in a spin pumping device without coupling to TSC by a rotating magnetic field, where low energy spin down electrons can be flipped to high energy spin up electrons by absorbing photons in the QD [62]. However, when one end of a TSC nanowire is coupled to the QD, a highly localized topological Andreev state is formed at the Fermi level even with weak coupling strength, which dominates the quantum transport of the spin pumping system. In this case, only electron pairs with opposite spin can be injected into the QD. By absorbing or emitting photons, this pair of electrons is separated and excited into opposite spin electrons, and then returns back to the lead again, generating an a.c. charge current without spin polarization. The switching from constant pure spin current to a.c. charge current suggests that spin pumping may be an effective method for detecting MZM in a TSC nanowire.

2 MZM involved spin pumping

We consider a spin-resolved three-probe system as shown in Fig. 1 where a QD is Ohmic-contacted by two semi-infinite leads and coupled to one end of a 1D topological superconductor nanowire. A rotating magnetic field is applied to the QD producing a spin resolved pumped current. The effective Hamiltonian of the

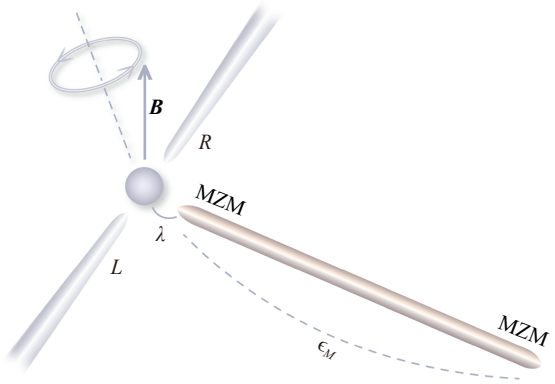

Fig. 1 Schematic structure of topological superconducting nanowire assisted spin pumping system. A rotating magnetic field ($\boldsymbol{B}$) is applied to the QD, and spin resolved quantum transport is measured through left (L) and right (R) semi-infinite metallic leads which are Ohmic-contacted to the QD. The QD is also coupled to one end of a topological superconducting nanowire with coupling strength equal to λ. MZMs indicate two zero energy modes located at both ends of the wire, and ϵ_M is the coupling strength between the two MZMs.

system can be written as [39, 62]

$$H = H_P + H_D + H_{DP} + H_B + H_M + H_{DM}, \tag{1}$$

where $H_P = \sum_{\alpha k} \epsilon_{\alpha k} c^\dagger_{\alpha k\sigma} c_{\alpha k\sigma}$ describes the spin resolved Hamiltonian of the left ($\alpha = L$) and right ($\alpha = R$) lead with $\sigma = \uparrow, \downarrow$ indicating the spin index. $H_D = \sum_\sigma \epsilon_d d^\dagger_\sigma d_\sigma$ represents spin degenerate single energy level of the isolated QD, where ϵ_d can be adjusted by a gate voltage. $H_{DP} = \sum_{\alpha k\sigma} t_{\alpha k\sigma} c^\dagger_{\alpha k\sigma} d_\sigma + H.c.$ refers to the coupling between the QD and two metallic leads. H_B describes a time-dependent driving potential due to a rotating magnetic field $\boldsymbol{B}(t) = B_0(\sin\theta\cos\omega t\boldsymbol{i} + \sin\theta\sin\omega t\boldsymbol{j} + \cos\theta\boldsymbol{k})$, where B_0 is the magnitude of magnetic field, θ is the angle between directions of the magnetic field and the rotation axis, and ω is the rotating frequency. The rotating magnetic field is crucial to generate a pure spin current. For example, a counter-clockwise rotating field allows a spin down electron to flip to spin up electron by absorbing a photon, but does not allow a spin up electron to flip to spin down electron by absorbing a photon, and thus the angular momentum is conserved. H_B is assumed to have the following form [62]

$$H_B = \kappa[\exp(-\mathrm{i}\omega t) d^\dagger_\uparrow d_\downarrow + \exp(\mathrm{i}\omega t) d^\dagger_\downarrow d_\uparrow]$$

with $\kappa = B_0 \sin\theta$ defining the effective magnetic field perpendicular to the rotation axis. These four terms give a minimal model of spin pumping as described in the previous study [62]. $H_M = \mathrm{i}\epsilon_M \gamma_1 \gamma_2/2$ is the Hamiltonian of the topological superconductor nanowire described by Kitaev model, where γ_1 and γ_2 are two Majorana operators obeying $\gamma_1\gamma_2 = -\gamma_2\gamma_1$ and $\gamma_m^2 = 1$. $\epsilon_M \sim \mathrm{e}^{-l/\xi}$ is the coupling strength between γ_1 and γ_2 with l the chain length and ξ the superconducting coherence length. $H_{DM} = \sum_\sigma (\lambda_\sigma d_\sigma - \lambda^*_\sigma d^\dagger_\sigma)\gamma_1$ is the coupling between the QD and the adjacent MZM, where $\lambda_\uparrow = \lambda$ and $\lambda_\downarrow = -\mathrm{i}\lambda$ indicate the coupling strength. The assumption of a real $\lambda_\uparrow$ and an imaginary $\lambda_\downarrow$ in this work is not arbitrary, which represents the same coupling strength and a different coupling phase [40]. By defining two new ordinary fermion operators $f = (\gamma_1 + \mathrm{i}\gamma_2)/2$ and $f^\dagger = (\gamma_1 - \mathrm{i}\gamma_2)/2$, H_M can be written as $H_M = \epsilon_M(f^\dagger f - \frac{1}{2})$, and H_{DM} can be written as $H_{DM} = \lambda(d_\uparrow - d^\dagger_\uparrow)(f + f^\dagger) - \mathrm{i}\lambda(d_\downarrow + d^\dagger_\downarrow)(f + f^\dagger)$.

In the adiabatic regime when ω is small, spin resolved current induced by rotating magnetic field from lead α to the QD can be calculated by [62]

$$I_{\alpha\sigma} = q\int \frac{\mathrm{d}E}{2\pi}(-\partial_E f)\mathrm{Tr}\left[\Gamma_\alpha G^r \mathrm{d}H' G^a\right]_{\sigma\sigma}, \tag{2}$$

where q is the charge quantity, Γ_α is the linewidth function describing the coupling between the leads and the QD, and $\mathrm{d}H' = \mathrm{d}H_B/\mathrm{d}t$. G^r is the non-equilibrium Green's function of the system, and the matrix elements $G^r_{\sigma\sigma'}$ related to the quantum transport are expressed as

$$G^r_{\sigma\sigma'} = \frac{1}{|A|}\begin{pmatrix} \left(E^2 - \frac{\epsilon_M^2}{4}\right)(E - \epsilon_2) - 2\lambda^2 E & -2\mathrm{i}\lambda^2 E + \kappa \mathrm{e}^{-\mathrm{i}\omega t}\left(E^2 - \frac{\epsilon_M^2}{4}\right) \\ 2\mathrm{i}\lambda^2 E + \kappa \mathrm{e}^{\mathrm{i}\omega t}\left(E^2 - \frac{\epsilon_M^2}{4}\right) & \left(E^2 - \frac{\epsilon_M^2}{4}\right)(E - \epsilon_1) - 2\lambda^2 E \end{pmatrix}_{\sigma\sigma'}, \tag{3}$$

where $\epsilon_{1,2} = \epsilon_d \pm B_0\cos\theta - \mathrm{i}\Gamma/2$ with $\Gamma = \Gamma_L + \Gamma_R$, and $A = [(E - \epsilon_1)(E - \epsilon_2) - \kappa^2](E^2 - \epsilon_M^2/4) - 2E(2E - \epsilon_1 - \epsilon_2)\lambda^2 - 4\lambda^2 E\kappa\sin(\omega t)$. By substituting $G^r_{\sigma\sigma'}$ into Eq. (2), in the low temperature limit, Eq. (2) is reduced to

$$I_{\alpha\sigma}(t) = \frac{q\Gamma_\alpha\omega\kappa}{2\pi|A_\mu|^2}\Big\{\left[4\lambda^2\mu\cos(\omega t)(\mu - \epsilon_d) + 2\sigma\lambda^2\mu\sin(\omega t)\Gamma\right] \times \left(\mu^2 - \frac{\epsilon_M^2}{4}\right) - 8\lambda^4\mu^2\cos(\omega t) + \sigma\kappa\Gamma\left(\mu^2 - \frac{\epsilon_M^2}{4}\right)^2\Big\}, \tag{4}$$

where μ is the chemical potential of the leads and $A_\mu \equiv A(E \to \mu)$. σ labels spin polarization $\uparrow/\downarrow$ and stands for ± 1 for electron energy. In the rest of this work, $I_{\alpha\sigma}$ is abbreviated as I_σ for simplicity.

Case I. We first consider the case of $\lambda = 0$, where Eq. (4) is reduced to

$$I_\uparrow \equiv -I_\downarrow = \frac{q\omega\Gamma_\alpha\Gamma\kappa^2}{2\pi|(\mu - \epsilon_1)(\mu - \epsilon_2) - \kappa^2|^2}, \tag{5}$$

which is accordant with that obtained in Ref. [62]. Obvi-

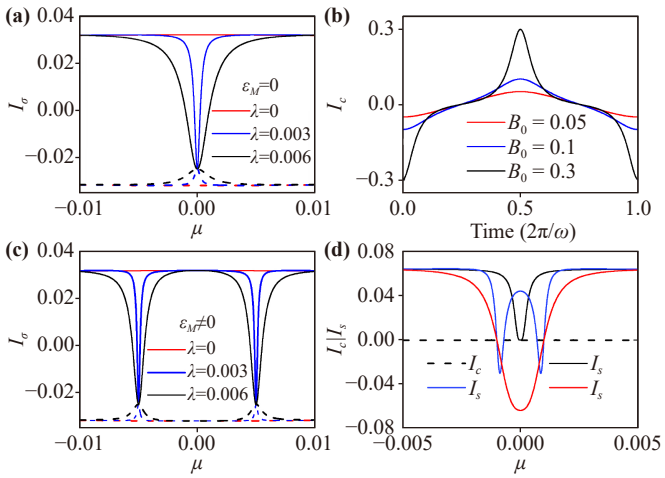

Fig. 2 **(a)** $I_\uparrow$ (solid curves) and $I_\downarrow$ (dash curves) versus μ with different λ when $\epsilon_M = 0$. The other parameters are $\epsilon_d = 0$, $\omega = 0.1$, $\theta = \pi/2$ and $\Gamma_L = \Gamma_R = 0.1$. **(b)** I_c versus time in one period of rotating magnetic field with different B_0 when $\lambda \neq 0$ and $\epsilon_M = 0$. **(c)** $I_\uparrow$ (solid curves) and $I_\downarrow$ (dash curves) versus μ with different λ when $\epsilon_M \neq 0$. Peaks appear at $\mu = \pm\epsilon_M/2$. **(d)** Ordinary fermion assisted I_c (black dashed line) and I_s (black solid curve) with $\lambda = 0.005$ and $\beta = 0$; I_s (blue solid curve) with $\lambda = 0.005$ and $\beta = 0.001$; I_s (red solid curve) with $\lambda = 0.01$ and $\beta = 0.001$. For (b–d), the other used parameters are the same as those in (a).

ously, the total charge current I_c $(= I_\uparrow + I_\downarrow)$ is zero and a pure spin current I_s $(= I_\uparrow - I_\downarrow)$ is generated. The pure spin current is time-independent, and its magnitude depends on the rotating magnetic field and the coupling strength between the QD and the leads.

Case II. We then consider the case of $\lambda \neq 0$ and $\epsilon_M = 0$. When $|\mu| \gg \lambda$, Eq. (4) is reduced to Eq. (5) meaning that spin pumping is not influenced by the MZM. However, when $\lambda \gg \mu$ which is easily satisfied if $\mu = 0$, Eq. (4) is simplified as

$$I_\uparrow(t) \equiv I_\downarrow(t) = -\frac{q\omega\Gamma_\alpha\kappa\cos(\omega t)}{4\pi[(\epsilon_d - \kappa\sin(\omega t))^2 + \Gamma^2/4]}, \tag{6}$$

which has two obvious differences compared with that of $\lambda = 0$. Firstly, $I_\uparrow$ is always equal to $I_\downarrow$ meaning a switching from pure spin current to charge current, and the charge current is independent of the magnitude of nonzero λ. Secondly, $I_\uparrow$ varies periodically with time, and the period is $2\pi/\omega$. Figure 2(a) shows $I_\uparrow$ (solid curves) and $I_\downarrow$ (dash curves) as functions of μ with different λ. When $\lambda = 0$, $I_\uparrow$ is always equal to $-I_\downarrow$ meaning a pure spin current. When $\lambda \neq 0$, $I_\uparrow$ falls and $I_\downarrow$ rises near $\mu = 0$. In particular, $I_\uparrow$ and $I_\downarrow$ reach the same value at $\mu = 0$ indicating a switching from pure spin current to charge current. The half widths of $I_\uparrow$ and $I_\downarrow$ peaks increase with λ, but the heights remain unchanged. It means that I_c is independent of the magnitude of λ at $\mu = 0$ as long as $\lambda \neq 0$. Figure 2(b) plots the time evolution of I_c under different magnetic field. We see that I_c increases firstly in the first half period and then decreases to the initial value in the second half period showing an inversion of current direction. The average current in one period is confirmed to be zero.

Case III. Finally, we consider the case of $\lambda \neq 0$ and $\epsilon_M \neq 0$. When $\mu \to 0$, Eq. (4) is reduced to Eq. (5) which is independent of the magnitude of ϵ_M. It means that the a.c. charge current with $\epsilon_M = 0$ is switched to a d.c. pure spin current again with $\epsilon_M \neq 0$. The same results can be obtained when $|\mu| \gg \lambda$ and $|\mu| \gg \epsilon_M$. However, when $\mu = \pm\epsilon_M/2$, Eq. (4) is reduced to

$$I_\uparrow \equiv I_\downarrow = -\frac{q\omega\Gamma_\alpha\kappa\cos(\omega t)}{4\pi[(\epsilon_d - \kappa\sin(\omega t) \mp \epsilon_M/2)^2 + \Gamma^2/4]}. \tag{7}$$

Obviously, an a.c. charge current occurs when $\mu = \pm\epsilon_M/2$. When $\epsilon_M \to 0$, Eq. (7) is reduced to Eq. (6). I_σ versus μ with different λ is given in Fig. 2(c) when $\epsilon_M \neq 0$. Compared with Fig. 2(a) where $\epsilon_M = 0$, the sharp peaks of I_σ move from $\mu = 0$ to $\mu = \pm\epsilon_M/2$. These two sharp peaks show similar information to Fig. 2(a), except that the peak width is halved. These features indicate that the MZM can always be detected by observing the switching from pure spin current to charge current, except that the chemical potential has to be shifted to $\pm\epsilon_M/2$.

To better understand the switching between pure spin current and charge current in the MZM coupled spin pumping system, we introduce a unitary transformation $U = \mathrm{e}^{\mathrm{i}\omega t/2(d_\uparrow^\dagger d_\uparrow - d_\downarrow^\dagger d_\downarrow)}$ to redefine the Hamiltonian of the system in the rotating reference as follows:

$$H_0^{RF} = U^\dagger H_0 U + \mathrm{i}\frac{\mathrm{d}U^\dagger}{\mathrm{d}t}U = \begin{pmatrix} \tilde{\epsilon}_{d\uparrow} & -\tilde{\lambda} & \kappa & -\tilde{\lambda} \\ -\tilde{\lambda}^* & \epsilon_M/2 & \mathrm{i}\tilde{\lambda}^* & 0 \\ \kappa & -\mathrm{i}\tilde{\lambda} & \tilde{\epsilon}_{d\downarrow} & -\mathrm{i}\tilde{\lambda} \\ -\tilde{\lambda}^* & 0 & \mathrm{i}\tilde{\lambda}^* & -\epsilon_M/2 \end{pmatrix}, \tag{8}$$

where $H_0 = H_D + H_B + H_M + H_{DM}$ represents the Hamiltonian of the MZM coupled QD with rotating magnetic field, and the matrix is defined with the basis set $[d_\uparrow, f, d_\downarrow, f^\dagger]$. $\tilde{\epsilon}_{d\sigma} = \epsilon_{d\sigma} + \sigma\omega/2$ and $\tilde{\lambda} = \lambda\mathrm{e}^{-\mathrm{i}\omega t/2}$. Obviously, an energy shift $\pm\omega/2$ occurs in the rotating reference for the spin up and spin down states of the QD, respectively. The influence from magnetic field becomes time-independent, while the coupling between the QD and the MZM evolves with time. The change of coupling explains the periodic oscillation of the charge current. Note that this transformation is not a strict derivation, as it is not started from the BdG representation. It serves only as a heuristic understanding to the oscillation of the charge current. The left panels of Fig. 3 illustrate the density of states (DOS) of the QD in a rotating reference under different conditions. The corresponding physical pictures of spin pumping are shown in the right panels of Fig. 3.

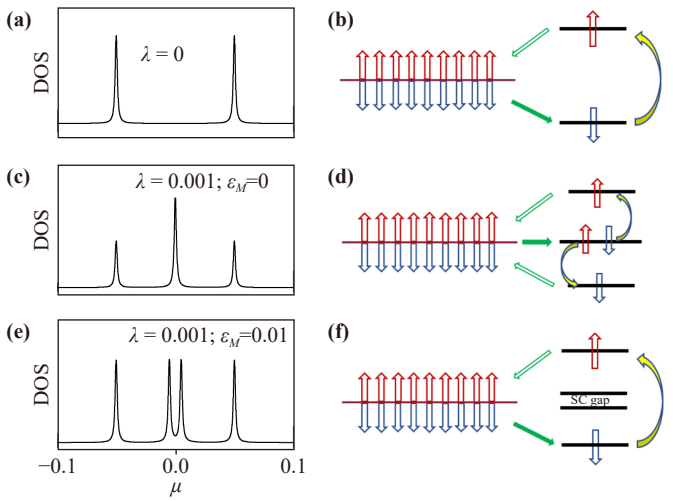

Fig. 3 DOS of the QD (left panels) and the corresponding schematic plot of MZM assisted spin pumping (right panels) when $\lambda = 0$ for **(a)** and **(b)**; $\lambda = 0.001$ and $\epsilon_M = 0$ for **(c)** and **(d)**; $\lambda = 0.001$ and $\epsilon_M = 0.01$ for **(e)** and **(f)**.

When $\lambda = 0$, two symmetrical spin states can be found at $E = \pm\omega/2$ in the QD, as depicted in Fig. 3(a). Despite equal coupling strengths between the lead and these two states, electrons from the left lead can only enter the low energy spin down state but not the high energy spin up state due to the selection rule of the rotating magnetic field. The spin down electrons are flipped to spin up electrons by absorbing photons, as demonstrated in Fig. 3(b), and then exit to the left lead again. The incoming spin down electrons and outgoing spin up electrons give rise to a pure spin current in the left lead. Considering of the symmetric coupling between the QD and two leads, the identical process occurs in the right lead and thus only the transport process in the left lead is presented in the right panels of Fig. 3. When $\lambda \neq 0$ but $\epsilon_M = 0$, a highly localized topological Andreev state is formed at $E = 0$ as shown in Fig. 3(c). This state dominates quantum transport of the spin pumping device when the incident electron's energy is zero. In this scenario, only electron pairs with opposite spin can access the zero energy level in the QD. The spin down electrons are excited to spin up electrons at the high energy level by absorbing photons, whereas the spin up electrons are flipped to spin down electrons at the low energy level by emitting photons as shown in Fig. 3(d). Eventually, the spin up and spin down electrons flow back to the lead again. As the coupling strength between the QD and MZM is time-dependent ($\tilde{\lambda} = \lambda e^{-i\omega t/2}$), the number of incoming electron pairs and outgoing electrons pairs also evolve with time, leading to the generation of an a.c. charge current [see Fig. 2(b)]. When the two MZMs are coupled ($\epsilon_M \neq 0$), the topological zero energy state disappears indicating a phase transition of the nanowire from a nontrivial TSC to an ordinary superconductor, and the highly localized topological Andreev state at $E = 0$ is split into two states at $\pm\epsilon_M/2$ as shown in Fig. 3(e). As the superconducting gap near $\mu = 0$ does not participate in electron transport, the device is reduced to the case of $\lambda = 0$, resulting in only pure spin current [see Fig. 3(f)]. As μ approaches the band edges of the superconducting gap $\pm\epsilon_M/2$, the Andreev bound states dominate the quantum transport again and charge current occurs as shown in Fig. 2(c).

To achieve the switching from pure spin current to charge current, it is essential to have equal coupling strength between the quantum dot and spin-resolved MZMs, i.e., $|\lambda_\uparrow| = |\lambda_\downarrow|$. However, due to the spin polarization of MZMs, this requires precise parameter tuning in experimental setups [63, 64]. To overcome this challenge, we couple the quantum dot to two MZMs at both ends of the superconducting nanowire simultaneously. Since the spin polarization of the MZM at the left end of the nanowire is opposite to that of the MZM at the right end, the spin up coupling strength $|\lambda_\uparrow|$ is equal to the spin down coupling strength $|\lambda_\downarrow|$ when the two MZMs are coupled to the quantum dot equally. Considering of the expression of H_{DM} in Eq. (1), it is clear that coupling to two MZMs with opposite spin polarization is equivalent to coupling to a spin-degenerate MZM with coupling strength doubled.

To investigate whether an ordinary fermion can also produce the switching from pure spin current to charge current, we coupled an ordinary fermion instead of a Majorana quasi-particle to the QD of the spin pumping device. The Hamiltonian of a minimal model is given by $H_{D'} = \sum_\sigma \epsilon'_{d\sigma} b^\dagger_\sigma b_\sigma + \beta b^\dagger_\sigma b_{\bar{\sigma}}$, and the coupling between two QDs is described by $H_{DD'} = \sum_\sigma \lambda d^\dagger_\sigma b_\sigma + H.c.$. When $\beta = \epsilon'_{d\sigma} = 0$, we find that the spin resolved current is given by $I_\sigma = \eta q \omega \Gamma_\alpha \Gamma \kappa^2 \mu^4/(2\pi|C|^2)$, where $C = [(\mu - \epsilon_d + i\Gamma/2)\mu - \lambda^2]^2 - \kappa^2\mu^2$. Interestingly, $I_\uparrow$ is equal in magnitude to $-I_\downarrow$ and remains time independent. However, when $\lambda \gg \mu \to 0$, both $I_\uparrow$ and $I_\downarrow$ approach to zero, indicating the absence of charge and spin current in the system [black dashed and solid curves in Fig. 2(d)]. As β increases, pure spin current gradually appears [blue and red solid curves in Fig. 2(d)], but no charge current is observed at any time. It is evident that the transport property produced by ordinary fermion-assisted spin pumping is entirely distinct from that produced by Majorana quasi-particle-assisted spin pumping. Hence, we conclude that the transition from pure spin current to charge current in quantum spin pumping provides an effective method to detect the presence of MZM.

3 Realistic TSC nanowire assisted spin pumping

To better comprehend the resilience of the MZM assisted spin pumping in actual physical devices, we replace the individual MZM with a more realistic TSC

nanowire, as outlined in Ref. [32],

$$
\begin{aligned}
&H_{wire} = H_0 + H_{soc} + H_{sc},\\
&H_0 = \sum_{i,\sigma}(-\mu + \eta V_z)C^{\dagger}_{i,\sigma}C_{i,\sigma} - \sum_{i,\sigma} tC^{\dagger}_{i,\sigma}C_{i+1,\sigma} + H.c.,\\
&H_{soc} = i\alpha_R \sum_{\mathrm{i},\sigma,\sigma'} C^{\dagger}_{i,\sigma}(\hat{x}\times\boldsymbol{\sigma})^{\sigma\sigma'}_{z} C_{i+1,\sigma'} + H.c.,\\
&H_{sc} = \Delta\sum_{i} C^{\dagger}_{i,\uparrow}C^{\dagger}_{i,\downarrow} + H.c..
\end{aligned}
\tag{9}
$$

H_0 describes the Hamiltonian of a finite-length nanowire. $C^{\dagger}_{i,\sigma}(C_{i,\sigma})$ generates (annihilates) an electron at site i with spin σ. μ is the chemical potential, and t is the coupling strength between the neighborhoods. V_z describes the Zeeman splitting regulated by an external magnetic field perpendicular to the nanowire. H_{soc} describes the Rashba spin–orbit coupling in the nanowire, where α_R represents the strength of spin–orbit interaction and $\boldsymbol{\sigma}$ is the Pauli matrix. H_{sc} describes the s-wave paring term with superconducting order parameter Δ arising from the superconducting proximity effect. The Bogoliubov–de Genes equation is formulated in the standard Nambu representation. When $V_z > \sqrt{\Delta^2+\mu^2}$, the superconducting nanowire enters the topological nontrivial phase accompanied by two MZMs at both ends of the nanowire. When $V_z < \sqrt{\Delta^2+\mu^2}$, the superconducting nanowire is in the topological trivial states. In our calculation, μ is fixed equal to zero, and a topological phase transition occurs at $V_z = \Delta$. Moreover, the nanowire is sufficiently long to ensure the decoupling between two MZMs.

Figures 4(a) and (b) display I_s and I_c as functions of μ, respectively, for the superconducting nanowire in its topological nontrivial phase (red curves and blue curves with $V_Z > \Delta$) and trivial phase (black curves with $V_Z < \Delta$). A weak coupling strength between the QD and the MZM is assumed to be $\lambda = t/50$. When $V_Z < \Delta$, I_s remains constant with respect to μ, and I_c remains zero. Conversely, when $V_Z > \Delta$, both I_s and I_c oscillate near $\mu = 0$. Moreover, I_s tends to zero while I_c remains finite when $\mu = 0$. For μ away from zero, I_s tends to constant, while I_c approaches zero. These results agree with those in Fig. 2, which illustrate that a side-coupled TSC nanowire can facilitate the switching from pure spin current to charge current in the spin pumping device. In Figs. 4(c) and (d), we present the evolution of I_c and I_s with different V_z and B_0 when $\mu = 0$. When the superconducting nanowire is in its topologically nontrivial phase with $V_Z > \Delta$, I_c oscillates with time for different B_0 with zero average current per cycle, while I_s remains perpetually zero, corroborating the findings in Fig. 2(a). Conversely, when $V_Z < \Delta$, I_c matches zero, and I_s oscillates against time. The differences in current information for $V_Z > \Delta$ and $V_Z < \Delta$ can serve to distinguish the topological phenomenon of a superconducting nanowire and verify the existence of MZM in 1D TSC.

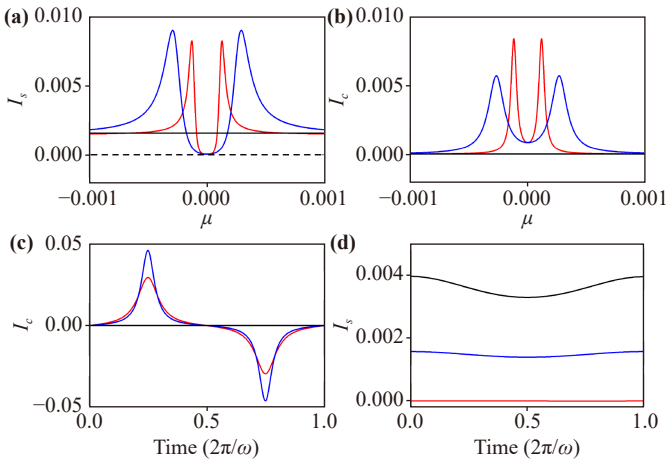

Fig. 4 I_s and I_c of the spin pumping device coupled by a TSC nanowire when $V_Z > \Delta$ or an ordinary superconducting nanowire when $V_Z < \Delta$. The fixed parameters are $\Delta = 0.04$, $\theta = \pi/2$, $\omega = 0.1$, $\Gamma_L = \Gamma_R = 0.1$, $\epsilon_d = 0$, $\alpha_R = 0.02$, and $\lambda = 0.002$. In **(a)** and **(b)**, B_0 is fixed to 0.05, and V_Z is changed to 0.06 (red curve), 0.05 (blue curve) and 0.03 (black curve). The dash line in (a) indicates the zero value. In **(c)** and **(d)**, both V_Z and B_0 are changed. In (c), (V_Z, B_0) is assumed to be the following values (0.05, 0.03) (red curve); (0.05, 0.05) (blue curve); (0.03, 0.05) (black curve). In (d), (V_Z, B_0) is assumed to be the following values (0.05, 0.05) (red curve); (0.03, 0.05) (blue curve); (0.03, 0.03) (black curve).

4 ps-ABSs assisted spin pumping

Previous studies have demonstrated that ps-ABSs in the superconducting nanowire-coupled QD systems can also exhibit the same $2e^2/h$ ZBCP behavior as induced by MZM in local quantum transport detection [42, 43]. When a nonuniform chemical potential emerges in the nanowire, a pair of ps-ABSs with quasi-zero energy can form at one end and the interior, even in the topologically trivial phase. When the QD is coupled to the ps-ABSs located at the end of the nanowire, ZBCP can also arise, which is robust in a wide range of Zeeman field and tunnel barrier height, potentially misleading the presence of MZM. In light of this, it is essential to clarify the influence of ps-ABSs on spin pumping. We consider a representative case to generate the ps-ABSs in a superconducting nanowire, as used in Ref. [42], where an additional long-range parabolic potential is included throughout the nanowire. The maximum value is set equal to Δ in the middle, and the minimum value is fixed to be zero at both ends of the nanowire, as depicted by the light-yellow filled image in Figs. 5(c) and (d).

Figure 5(a) illustrates the eigenvalues of the supercon-

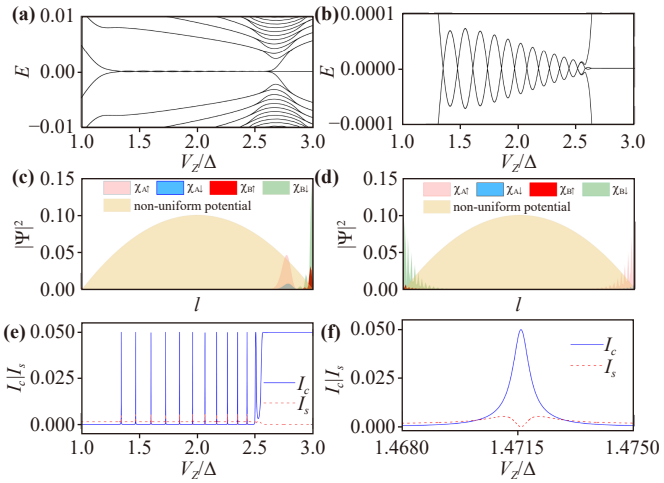

Fig. 5 ps-ABSs assisted spin pumping. **(a)** Energy spectrum of a superconducting nanowire with a long-range parabolic potential versus V_z/Δ; **(b)** zoom in of (a) near the quasi-zero modes; **(c)** distribution of a pair of ps-ABSs ξ_A and ξ_B at $V_Z/\Delta = 1.475$; **(d)** distribution of a pair of MZMs ξ_A and ξ_B at $V_Z/\Delta = 3.0$. In (c) and (d), the light-yellow covered region from left to right describes the parabolic potential with maximum value equal to Δ. **(e)** I_s and I_c of the spin pumping device coupled by one end of superconducting nanowire with V_Z/Δ; **(f)** I_s and I_c at one of the sharp peak in (e). The black dash line indicates the zero value. The parameters are $V_Z/\Delta = 1.472$.

ducting nanowire including the parabolic potential with increasing Zeeman splitting. As V_Z/Δ increases, the band gap gradually closes at approximately 1.3, and quasi-zero modes emerge in a wide range from around 1.3 to 2.6. Each quasi-zero mode corresponds to a pair of ps-ABSs consisting of two overlapping MBSs with separation on the order of the Majorana decay length ξ, where the system remains in the topological trivial state. With further increase of V_Z/Δ beyond 2.6, the system enters the topological nontrivial states, and MZMs appear at the ends of the nanowire. It is important to note that the criterion of topological phase transition is no longer the simple relation between V_z and $\sqrt{\Delta^2+\mu^2}$ due to the presence of the non-uniform potential. The details of the quasi-zero modes are amplified in Fig. 3(b), and each cross corresponds to a pair of ABSs at $E = 0$, consistent with the finding in Refs. [42, 43]. Correspondingly, the topological trivial ps-ABSs at $V_Z/\Delta = 1.5$ and topological nontrivial MZMs at $V_Z/\Delta = 2.8$ are depicted in Figs. 5(c) and (d), respectively, where the ps-ABSs overlap at one end of the nanowire, while two MZMs appear at both ends.

Figure 5(e) plots the pumping current I_c and pure spin current I_s against V_Z/Δ from the topological trivial to nontrivial region. When $V_Z/\Delta < 1.3$, I_c remains at zero, and a d.c. pure spin current I_s is present, consistent with the case of topological trivial phase without the non-uniform potential, as shown in Fig. 2. As V_Z/Δ changes from 1.3 to 2.6, a series of sharp peaks in I_c appear, accompanied by disappearance of I_s. To see the peaks more clearly, one of them is amplified in Fig. 5(f). We observe that I_c tends to zero with finite I_s away from the peak, while I_s is equal to zero with finite I_c at the peak, signifying a switch from pure spin current to charge current. Moreover, this switch only occurs at the cross points in Fig. 5(b) where the energy of the ps-ABSs is precisely zero. With further increase of V_Z/Δ beyond 2.6, a plateau of I_c appears, accompanied by $I_s = 0$. The plateau remains stable over a wide range of V_Z/Δ with value equal to that of the peaks, corresponding to a topological phase transition from trivial to nontrivial states of the superconducting nanowire, or in other words, the presence of MZMs. We also investigated other nonuniform potentials, such as a short parabolic potential as used in Ref. [42], and found that only the ps-ABSs with precisely zero energy can switch the pure spin current to charge current like MZMs. However, this switch is extremely unstable and highly sensitive to the Zeeman field, providing a method to distinguish between zero-energy ps-ABSs and MZMs. This is different from the case of ZBCP, where the induced ZBCP by ps-ABSs and MZMs is indistinguishable over a wide range of Zeeman field in local charge tunneling experiments [42]. Our investigation suggests that spin pumping could potentially be an effective method for detecting the presence of MZMs at the ends of a TSC nanowire. However, the proposed scheme is upon a simple theoretical model, and there are still many issues to be addressed, such as model simplification, experimental feasibility, and the potential impact of other factors on the spin pumping process. Further theoretical and experimental studies are required to fully elucidate this concept.

5 Expending discussion

Next, we give a brief discuss to this study from the perspective of decoherence, shot noise and experimental implementation, aiming to gain a deeper understanding and broader application of the MZM assisted spin pumping.

Decoherence is a fundamental phenomenon resulting from inelastic scattering in quantum transport, which can be effectively modeled using a phenomenological approach by involving a hypothetical probe [65]. It is equivalent to appending an additional virtual self-energy term $\Sigma_v^r = i\eta$ into G^r of the system, where η represents the dephasing parameter. Notably, the presence of this virtual self-energy term solely modifies the value of Γ_α in Eq. (4), without altering other parameters. In essence, decoherence exclusively modifies the magnitude of the spin-resolved current, leaving the characteristic behavior of MZM assisted spin pumping unaltered, where the pure spin current transitions to charge current.

Shot noise originates from the particle nature of elec-

trons, which has been thoroughly explored in quantum transport systems [66–68]. By quantifying shot noise, we can identify the quasi-particle's spin or charge unit. In quantum spin pumping, both cross- and auto-correlation measurements are crucial for characterizing spin current noise. Despite the absence of a net charge current, a shot noise in charge current persists due to the counterbalancing flow of spin up and spin down electrons. The emergence of MZM transforms spin correlations into charge correlations, potentially offering richer quantum insights. Consequently, a thorough examination of spin noise in MZM assisted spin pumping systems is imperative in future research.

Although this work provides a theoretical framework for exploring the MZM assisted spin pumping, we maintain an optimistic perspective for its experimental realization. Spin pumping devices have been successfully demonstrated across various platforms, including GaAs/AlGaAs two-dimensional electron gas systems that utilize electron-beam patterned CrAu depletion gates and nonmagnetic PtAuGe Ohmic contacts [69]. However, the successful fabrication of the 1D TSC remains a notable challenge in experimental settings. Despite this, given the firmly established theory of MZMs, we continue to anticipate that the unambiguous observation of MZMs in experiments, along with the achievement of integrated measurements with spin pumping devices, will be feasible with the advancements in experimental technology.

6 Summary

In summary, we investigated the spin pumping effect influenced by MZMs at the end of a TSC nanowire. Even a very weak coupling between the QD and the adjacent MZM can change the d.c. pure spin current in the pumping system to time-dependent charge current when the chemical potential is equal to zero. However, when the superconducting nanowire is at the topological trivial state, the a.c. charge current reverts to d.c. pure spin current again. Although the ps-ABSs with precise zero energy can also switch the pure spin current to charge current, it is extremely unstable and highly sensitive to the Zeeman field, which is different from the MZMs assisted switching. Our investigation suggests that spin pumping could potentially be an effective method for detecting the presence of MZMs at the ends of a TSC nanowire.

Declarations The authors declare that they have no competing interests and there are no conflicts.

Acknowledgements This work was supported by the National Natural Science Foundation of China (Grant No. 12034014) and the Shenzhen Natural Science Foundation (Grant No. 20231120172734001). The authors thank Z. R. Gong and Z. F. Jiang for useful discussions.

References

1. F. Wilczek, Majorana returns, *Nat. Phys.* 5(9), 614 (2009)
2. J. Alicea, New directions in the pursuit of Majorana fermions in solid state systems, *Rep. Prog. Phys.* 75(7), 076501 (2012)
3. C. W. J. Beenakker, Search for Majorana fermions in superconductors, *Annu. Rev. Condens. Matter Phys.* 4(1), 113 (2013)
4. H. M. Guo, A brief review on one-dimensional topological insulators and superconductors, *Sci. China Phys. Mech. Astron.* 59(3), 637401 (2016)
5. M. Sato and Y. Ando, Topological superconductors: A review, *Rep. Prog. Phys.* 80(7), 076501 (2017)
6. D. Culcer, A. C. Keser, Y. Li, and G. Tkachov, Transport in two-dimensional topological materials: Recent developments in experiment and theory, *2D Mater.* 7, 022007 (2020)
7. Q. Zhang and B. Wu, Majorana modes in solid state systems and its dynamics, *Front. Phys.* 13(2), 137101 (2018)
8. M. He, H. Sun, and Q. L. He, Topological insulator: Spintronics and quantum computations, *Front. Phys.* 14(4), 43401 (2019)
9. D. Aoki, J. P. Brison, J. Flouquet, K. Ishida, G. Knebel, Y. Tokunaga, and Y. Yanase, Unconventional Superconductivity in UTe_2, *J. Phys.: Condens. Matter* 34(24), 243002 (2022)
10. S. K. Ghosh, M. Smidman, T. Shang, J. F. Annett, A. D. Hillier, J. Quintanilla, and H. Q. Yuan, Recent progress on superconductors with time-reversal symmetry breaking, *J. Phys.: Condens. Matter* 33(3), 033001 (2021)
11. E. Prada, P. San-Jose, M. W. A. de Moor, A. Geresdi, E. J. H. Lee, J. Klinovaja, D. Loss, J. Nygard, R. Aguado, and L. P. Kouwenhoven, From Andreev to Majorana bound states in hybrid superconductor–semiconductor nanowires, *Nat. Rev. Phys.* 2(10), 575 (2020)
12. Z. H. Wang, F. Xu, L. Li, D. H. Xu, and B. Wang, Topological superconductors and exact mobility edges in non-Hermitian quasicrystals, *Phys. Rev. B* 105(2), 024514 (2022)
13. Z. H. Wang, F. Xu, L. Li, D. H. Xu, W. Q. Chen, and B. Wang, Majorana polarization in non-Hermitian topological superconductors, *Phys. Rev. B* 103(13), 134507 (2021)
14. A. Y. Kitaev, Unpaired Majorana fermions in quantum wires, *Phys. Uspekhi* 44(10S), 131 (2001)
15. D. A. Ivanov, Non-Abelian statistics of half-quantum vortices in p-wave superconductors, *Phys. Rev. Lett.* 86(2), 268 (2001)
16. S. Ran, C. Eckberg, Q. P. Ding, Y. Furukawa, T. Metz, S. R. Saha, I. L. Liu, M. Zic, H. Kim, J. Paglione, and N. P. Butch, Nearly ferromagnetic spin-triplet superconductivity, *Science* 365(6454), 684 (2019)
17. M. Novak, S. Sasaki, M. Kriener, K. Segawa, and Y. Ando, Unusual nature of fully gapped superconductivity in In-doped SnTe, *Phys. Rev. B* 88, 140502(R) (2013)
18. L. Fu and C. L. Kane, Superconducting proximity effect

and majorana fermions at the surface of a topological insulator, *Phys. Rev. Lett.* 100(9), 096407 (2008)
19. R. M. Lutchyn, J. D. Sau, and S. Das Sarma, Majorana fermions and a topological phase transition in semiconductor–superconductor heterostructures, *Phys. Rev. Lett.* 105(7), 077001 (2010)
20. Y. Oreg, G. Refael, and F. von Oppen, Helical liquids and Majorana bound states in quantum wires, *Phys. Rev. Lett.* 105(17), 177002 (2010)
21. V. Mourik, K. Zuo, S. M. Frolov, S. R. Plissard, E. P. A. M. Bakkers, and L. P. Kouwenhoven, Signatures of Majorana fermions in hybrid superconductor–semiconductor nanowire devices, *Science* 336(6084), 1003 (2012)
22. M. Deng, C. Yu, G. Huang, M. Larsson, P. Caroff, and H. Xu, Anomalous zero-bias conductance peak in a NbCInSb nanowire–Nb hybrid device, *Nano Lett.* 12(12), 6414 (2012)
23. A. Das, Y. Ronen, Y. Most, Y. Oreg, M. Heiblum, and H. Shtrikman, Zero-bias peaks and splitting in an AlCInAs nanowire topological superconductor as a signature of Majorana fermions, *Nat. Phys.* 8(12), 887 (2012)
24. L. P. Rokhinson, X. Liu, and J. K. Furdyna, The fractional a.c. Josephson effect in a semiconductor–superconductor nanowire as a signature of Majorana particles, *Nat. Phys.* 8(11), 795 (2012)
25. H. O. H. Churchill, V. Fatemi, K. Grove-Rasmussen, M. T. Deng, P. Caroff, H. Q. Xu, and C. M. Marcus, Superconductor–nanowire devices from tunneling to the multichannel regime: Zero-bias oscillations and magnetoconductance crossover, *Phys. Rev. B* 87(24), 241401 (2013)
26. A. D. K. Finck, D. J. Van Harlingen, P. K. Mohseni, K. Jung, and X. Li, Anomalous modulation of a zero-bias peak in a hybrid nanowire–superconductor device, *Phys. Rev. Lett.* 110(12), 126406 (2013)
27. S. M. Albrecht, A. P. Higginbotham, M. Madsen, F. Kuemmeth, T. S. Jespersen, J. Nygard, P. Krogstrup, and C. M. Marcus, Exponential protection of zero modes in Majorana islands, *Nature* 531(7593), 206 (2016)
28. S. Nadj-Perge, I. K. Drozdov, J. Li, H. Chen, S. Jeon, J. Seo, A. H. MacDonald, B. A. Bernevig, and A. Yazdani, Observation of Majorana fermions in ferromagnetic atomic chains on a superconductor, *Science* 346(6209), 602 (2014)
29. R. Pawlak, M. Kisiel, J. Klinovaja, T. Meier, S. Kawai, T. Glatzel, D. Loss, and E. Meyer, Probing atomic structure and Majorana wavefunctions in mono-atomic Fe chains on superconducting Pb surface, *npj Quantum Inf.* 2, 16035 (2016)
30. Z. H. Wang, F. Xu, L. Li, D. H. Xu, W. Q. Chen, B. Wang, and H. Guo, Spin–orbit proximity effect and topological superconductivity in graphene/transition-metal dichalcogenide nanoribbons, *New J. Phys.* 23(12), 123002 (2021)
31. Z. H. Wang, F. Xu, L. Li, D. H. Xu, W. Q. Chen, and B. Wang, Majorana polarization in non-Hermitian topological superconductors, *Phys. Rev. B* 103(13), 134507 (2021)
32. Z. H. Wang, F. Xu, L. Li, R. Lü, B. Wang, and W. Q. Chen, One-dimensional topological superconductivity at the edges of twisted bilayer graphene nanoribbons, *Phys. Rev. B* 100(9), 094531 (2019)
33. K. T. Law, P. A. Lee, and T. K. Ng, Majorana fermion induced resonant Andreev reflection, *Phys. Rev. Lett.* 103(23), 237001 (2009)
34. J. P. Xu, M. X. Wang, Z. L. Liu, J. F. Ge, X. Yang, C. Liu, Z. A. Xu, D. Guan, C. L. Gao, D. Qian, Y. Liu, Q. H. Wang, F. C. Zhang, Q. K. Xue, and J. F. Jia, Experimental detection of a Majorana mode in the core of a magnetic vortex inside a topological insulator–superconductor $Bi_2Te_3/NbSe_2$ heterostructure, *Phys. Rev. Lett.* 114(1), 017001 (2015)
35. W. DeGottardi, D. Sen, and S. Vishveshwara, Majorana fermions in superconducting 1D systems having periodic, quasiperiodic, and disordered potentials, *Phys. Rev. Lett.* 110(14), 146404 (2013)
36. I. Adagideli, M. Wimmer, and A. Teker, Effects of electron scattering on the topological properties of nanowires: Majorana fermions from disorder and superlattices, *Phys. Rev. B* 89(14), 144506 (2014)
37. J. Liu, A. C. Potter, K. T. Law, and P. A. Lee, Zero-bias peaks in the tunneling conductance of spin–orbit-coupled superconducting wires with and without majorana end-states, *Phys. Rev. Lett.* 109(26), 267002 (2012)
38. D. I. Pikulin, J. P. Dahlhaus, M. Wimmer, H. Schomerus, and C. W. J. Beenakker, A zero-voltage conductance peak from weak antilocalization in a Majorana nanowire, *New J. Phys.* 14(12), 125011 (2012)
39. D. E. Liu and H. U. Baranger, Detecting a Majorana-fermion zero mode using a quantum dot, *Phys. Rev. B* 84, 201308(R) (2011)
40. M. Leijnse and K. Flensberg, Scheme to measure Majorana fermion lifetimes using a quantum dot, *Phys. Rev. B* 84, 140501(R) (2011)
41. H. Zhang, C. X. Liu, S. Gazibegovic, D. Xu, J. A. Logan, G. Wang, N. van Loo, J. D. S. Bommer, M. W. A. de Moor, D. Car, R. L. M. Op het Veld, P. J. van Veldhoven, S. Koelling, M. A. Verheijen, M. Pendharkar, D. J. Pennachio, B. Shojaei, J. S. Lee, C. J. Palmstrøm, E. P. A. M. Bakkers, S. D. Sarma, and L. P. Kouwenhoven, Retracted article: Quantized Majorana conductance, *Nature* 556(7699), 74 (2018)
42. C. Moore, T. D. Stanescu, and S. Tewari, Two-terminal charge tunneling: Disentangling Majorana zero modes from partially separated Andreev bound states in semiconductor–superconductor heterostructures, *Phys. Rev. B* 97(16), 165302 (2018)
43. C. Moore, C. C. Zeng, T. D. Stanescu, and S. Tewari, Quantized zero-bias conductance plateau in semiconductor –superconductor heterostructures without topological Majorana zero modes, *Phys. Rev. B* 98(15), 155314 (2018)
44. Y. Mao and Q. F. Sun, Charge and spin transport through a normal lead coupled to an *s*-wave superconductor and a Majorana zero mode, *Phys. Rev. B* 103(11), 115411 (2021)
45. S. K. Watson, R. M. Potok, C. M. Marcus, and V. Umansky, Experimental realization of a quantum spin pump, *Phys. Rev. Lett.* 91(25), 258301 (2003)
46. Y. Tserkovnyak, A. Brataas, and G. E. W. Bauer, Enhanced Gilbert damping in thin ferromagnetic films,

Phys. Rev. Lett. 88(11), 117601 (2002)
47. S. Dushenko, H. Ago, K. Kawahara, T. Tsuda, S. Kuwabata, T. Takenobu, T. Shinjo, Y. Ando, and M. Shiraishi, Gate-tunable spin-charge conversion and the role of spin–orbit interaction in graphene, *Phys. Rev. Lett.* 116(16), 166102 (2016)
48. K. Uchida, H. Adachi, T. An, T. Ota, M. Toda, B. Hillebrands, S. Maekawa, and E. Saitoh, Long-range spin Seebeck effect and acoustic spin pumping, *Nat. Mater.* 10(10), 737 (2011)
49. M. Weiler, M. Althammer, F. D. Czeschka, H. Huebl, M. S. Wagner, M. Opel, I. Imort, G. Reiss, A. Thomas, R. Gross, and S. T. B. Goennenwein, Local charge and spin currents in magnetothermal landscapes, *Phys. Rev. Lett.* 108(10), 106602 (2012)
50. H. Adachi and S. Maekawa, Theory of the acoustic spin pumping, *Solid State Commun.* 198, 22 (2014)
51. O. Mosendz, J. E. Pearson, F. Y. Fradin, G. E. W. Bauer, S. D. Bader, and A. Hoffmann, Quantifying spin Hall angles from spin pumping: Experiments and theory, *Phys. Rev. Lett.* 104(4), 046601 (2010)
52. C. W. Sandweg, Y. Kajiwara, A. V. Chumak, A. A. Serga, V. I. Vasyuchka, M. B. Jungfleisch, E. Saitoh, and B. Hillebrands, Spin pumping by parametrically excited exchange magnons, *Phys. Rev. Lett.* 106(21), 216601 (2011)
53. F. D. Czeschka, L. Dreher, M. S. Brandt, M. Weiler, M. Althammer, I. M. Imort, G. Reiss, A. Thomas, W. Schoch, W. Limmer, H. Huebl, R. Gross, and S. T. B. Goennenwein, Scaling behavior of the spin pumping effect in ferromagnet-platinum bilayers, *Phys. Rev. Lett.* 107(4), 046601 (2011)
54. S. Dushenko, M. Koike, Y. Ando, T. Shinjo, M. Myronov, and M. Shiraishi, Experimental demonstration of room-temperature spin transport in n-type germanium epilayers, *Phys. Rev. Lett.* 114(19), 196602 (2015)
55. K. Ando, S. Takahashi, J. Ieda, H. Kurebayashi, T. Trypiniotis, C. H. W. Barnes, S. Maekawa, and E. Saitoh, Electrically tunable spin injector free from the impedance mismatch problem, *Nat. Mater.* 10(9), 655 (2011)
56. Z. Tang, E. Shikoh, H. Ago, K. Kawahara, Y. Ando, T. Shinjo, and M. Shiraishi, Dynamically generated pure spin current in single-layer graphene, *Phys. Rev. B* 87(14), 140401 (2013)
57. J. B. S. Mendes, A. Aparecido-Ferreira, J. Holanda, A. Azevedo, and S. M. Rezende, Efficient spin to charge current conversion in the 2D semiconductor MoS_2 by spin pumping from yttrium iron garnet, *Appl. Phys. Lett.* 112(24), 242407 (2018)
58. A. A. Zvyagin, Longitudinal spin pumping and topological superconductivity: Search for Majorana edge states, *Phys. Rev. B* 89(21), 214420 (2014)
59. A. A. Zvyagin, Dynamics of the Kitaev chain model under parametric pumping, *Phys. Rev. B* 90(1), 014507 (2014)
60. A. A. Zvyagin, Modulation of the longitudinal pumping in quantum spin systems, *Phys. Rev. B* 101(17), 174408 (2020)
61. V. F. Becerra, M. Trif, and T. Hyart, Quantized spin pumping in topological ferromagnetic-superconducting nanowires, *Phys. Rev. Lett.* 130(23), 237002 (2023)
62. B. G. Wang, J. Wang, and H. Guo, Quantum spin field effect transistor, *Phys. Rev. B* 67(9), 092408 (2003)
63. E. Prada, R. Aguado, and P. San-Jose, Measuring Majorana nonlocality and spin structure with a quantum dot, *Phys. Rev. B* 96(8), 085418 (2017)
64. Ö. M. Aksoy and J. R. Tolsma, Majorana zero modes in a quantum wire platform without Rashba spin–orbit coupling, *Phys. Rev. B* 101(19), 195127 (2020)
65. M. Büttiker, Role of quantum coherence in series resistors, *Phys. Rev. B* 33(5), 3020 (1986)
66. B. G. Wang, J. Wang, and H. Guo, Shot noise of spin current, *Phys. Rev. B* 69(15), 153301 (2004)
67. B. Dong, H. L. Cui, and X. L. Lei, Pumped spin-current and shot-noise spectra of a single quantum dot, *Phys. Rev. Lett.* 94(6), 066601 (2005)
68. M. Matsuo, Y. Ohnuma, T. Kato, and S. Maekawa, Spin current noise of the spin Seebeck effect and spin pumping, *Phys. Rev. Lett.* 120(3), 037201 (2018)
69. S. K. Watson, R. M. Potok, C. M. Marcus, and V. Umansky, Experimental realization of a quantum spin pump, *Phys. Rev. Lett.* 91(25), 258301 (2003)